Mongolian Journal of Chemistry
www.mongoliajol.info/index.php/MJC

Enhanced energy storage: Electrochemical performance of $ZnCl_2$-activated carbon derived from *Acacia catechu* Bark

Pawan Kumar Mishra[1,2,3], Sabin Aryal[2], Hari Bhakta Oli[2], Timila Shrestha[2], Md Al Mamun[4], Ram Lal Swagat Shrestha[2]*, Deval Prasad Bhattarai[2]*

[1]*Department of Chemistry, Tri-Chandra Multiple Campus, Tribhuvan University, Kathmandu 44600, Nepal*
[2]*Department of Chemistry, Amrit Campus, Tribhuvan University, Kathmandu 44600, Nepal*
[3]*Central Department of Chemistry, Kirtipur, Tribhuvan University, Kathmandu 44600 Nepal*
[4]*Department of Atomic energy center, Materials Science Division, Dhaka 1000, Bangladesh*

* *Corresponding author: devalprasadbhattarai@gmail.com;* ORCID: https: https://orcid.org/0000-0002-2900-7674

Received: 26 June 2024; revised: 4 November 2024 ; accepted: 22 November 2024

ABSTRACT

In this study, *Acacia catechu* bark was used for the development of advanced supercapacitor negatrode materials through the synthesis of activated carbon via activation and carbonization at varying temperatures (400, 600, 800°C) using zinc chloride ($ZnCl_2$) as the activating agent. The as-prepared sample was characterized using X-ray diffraction (XRD), Fourier-transform infrared (FTIR) techniques. The specific surface area was evaluated using Brunauer-Emmet-Teller (BET) analysis, while 3D morphological assembly of the resulting material was assessed by means of the Field Emission Scanning Electron Microscopy. Cyclic voltammetry, galvanostatic charging and discharging, electrochemical impedance, were conducted to evaluate the material's electrochemical performance. The activated carbon prepared at 800°C (BZAC-8) exhibited a specific capacitance of 259.34 F g^{-1} at a current density of 1 A g^{-1} with excellent capacity retention (92.61 %) and lower impedance. These findings underscore the potential of utilizing *Acacia catechu* bark-based active carbon as a negatrode material for advanced energy-storing application.

Keywords: *Acacia catechu bark*, activated carbon, bio-waste, negatrode, supercapacitor

INTRODUCTION

The cumulative petition for efficient and sustainable energy stowing solutions has compelled extensive research into the development of high-performance supercapacitors [1]. Supercapacitors are electrochemical gadgets that store energy via electrostatic double layer capacitance and electrochemical pseudocapacitance, offering extraordinary power, elongated cycle lifespan, and swift charging-discharging capabilities [2]. Regardless of the plentiful welfares allied with commercialization of supercapacitor (SC), its extensive adoption is impeded by relatively truncated energy density and the inflated costs involved in their production [3]. The energy-storing ability of a supercapacitor is influenced by several factors, including the properties of electrode materials, the composition of electrolyte, the interaction between electrode-electrolyte, fabrication process, and ambient conditions [4].

The classification of supercapacitors is predominantly based on the working mechanism and composition of the electrode materials [5]. The three prime types of supercapacitors are electrochemical double-layer capacitors (EDLCs), pseudocapacitors, and hybrid capacitors [6]. EDLCs employ carbonaceous constituents for instance carbon nanotubes (CNTs) graphene materials, and activated carbons, which store energy through electrostatic mechanisms [7]. In contrast, pseudocapacitors apply materials like conducting polymers and transition metal oxides/phosphides/sulfides that facilitate energy-storage through Faradaic reactions [8]. Hybrid supercapacitors, on the other hand, combine the competences of EDLC materials with those of pseudocapacitive or battery-type materials to augment overall performance [9]. While pseudocapacitors and hybrid supercapacitors unveil higher capacitance and energy density, they are limited by their cyclic stability and rate capability [3,10].

Furthermore, the production process and disposal of pseudocapacitive and hybrid materials pose potential health risks due to the prevalent use of transition metals or their composites [11]. In light of these concerns, activated carbon derived from biomass sources is considered the ideal material for energy-storage applications due to its sustainability and safety profile [12,13].

The pursuit of sustainable and high-performance supercapacitor electrodes has led to the exploration of various carbonaceous materials [14]. Among these, activated carbon (AC) has emerged as an ideal choice for EDLC materials due to its high specific surface area, tunable pore structure, and excellent electrical conductivity, offering a balance between energy-storage and power delivery [15]. The idealness of porous activated carbon materials is attributed to the ease of synthesis, affordability, well-established production methodologies, and ability to form a reversible double layer, enhancing capacitive stability [16]. Biomass-derived activated carbon has garnered significant attention as a cost-effective and environmentally friendly alternative to conventional AC precursors [17].

Acacia catechu, a tree native to parts of Asia, produces a bark that is rich in tannins and other phytochemicals [18]. The bark has been traditionally used in various applications, such as medicine and dye production [19]. However, the potential of *Acacia catechu* bark as a precursor for activated carbon has not been extensively explored. In this research, synthesis of $ZnCl_2$-activated carbon derived from *Acacia catechu* bark and its application as an electrode material for supercapacitors is reported. The use of $ZnCl_2$ as an activator has been shown to enhance the porosity and electrical conductivity of activated carbon, leading to improved electrochemical performance of BZAC-8 with specific capacitance of 259.34 F g^{-1} at 1 A g^{-1}. This higher capacitance is due to the nanoporous structure with specific surface area of 1947 m^2 g^{-1}, and graphitic nature as disclosed from Raman spectra. These results demonstrate the potential of *Acacia catechu* bark-derived activated carbon at optimum temperature of 800°C (BZAC-8) as an exorbitant-performing electrode for energy harvesting purpose, as compared to counter samples (BZAC-6, and BZAC-4).

EXPERIMENTAL

Sample Collection and Pre-carbonization Process: The ***Acacia catechu*** bark harvested from the Garambesi, Rainas-7, Lumjung district, Nepal was reduced to tiny fragments and subjected to shade drying after that ground into a fine powder using an Herbal Medicine Disintegrator (FW 177). The powder was sieved to ensure the consistency of the particulate size then reserved for pre-carbonization process. A mass of 50 grams of the finely powdered bark material was accurately weighed using a digital balance. This powder was placed in a silicon basin and introduced into a muffle furnace, where it was subjected to heat treatment at 280°C for three hours. The material obtained after this process is termed as "pre-carbonized precursor" and denoted as BZAC-0.

Activation and Carbonization of the Material: A mixture consisting of 5 grams of pre-carbonized bark powder and an equal mass of $ZnCl_2$ was thoroughly mixed by continuous grinding for two hours in an agate mortar to produce a homogeneous fine paste. This paste was subsequently transferred to a ceramic boat and allowed to rest at ambient temperature for a period of 24 hours. Following this, the boat was placed in a tube furnace to initiate the carbonization process at varying temperatures of 400°C, 600°C and 800°C under a nitrogen atmosphere. After the carbonization, the material was once again ground to achieve a homogeneous mixture. The solution was continually washed using distilled water till a neutral pH was attained. The resultant material was ground in an agate mortar to obtain a fine powder suitable for characterization. The activated carbon samples prepared at carbonization temperatures of 400°C, 600°C and 800°C were labeled as BZAC-4, BZAC-6 and BZAC-8, respectively. The experimental procedure is illustrated in the Scheme 1.

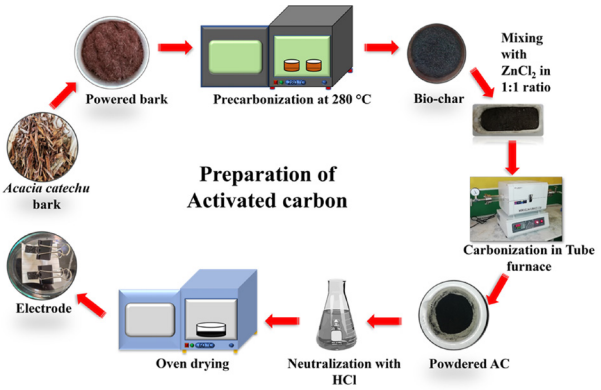

Scheme 1. Experimental procedure for the synthesis of activated carbon from *Acacia catechu* bark using $ZnCl_2$.

Materials Characterization: Fourier-Transform Infrared (FTIR) was utilized to ascertain the active groups existing in the activated carbon (BZAC). Spectra were recorded using a Perkin Elmer FTIR spectrometer (Spectrum IR version 10.6.2) located at Amrit Campus, Nepal, operating in Attenuated Total Reflection (ATR) approach through a wavenumber array of 4000 to 400 cm^{-1} at room temperature (25°C). X-ray diffraction (XRD) spectra of the powdered samples were attained utilizing a Rigaku Diffractometer, operating at 40 kV and 40 mA with a CuKα radiation source (λ = 1.54059 Å). The measurements were conducted at a scanning rate of 3° per minute over a 2θ range of 10-80°. The surface morphology and compositional elements of the activated carbon were inspected by means of a Field-Emission Scanning Electron Microscope (FESEM,

JEOL-FE version-2 instrument JSM-IT 800, USA). The specific surface area and pore volume of the samples were determined using Brunauer-Emmett-Teller (BET) and Barret-Joyner-Halenda (BJH) method, respectively on a Quantachrome Instruments (v3.01). The sample was investigated using nitrogen adsorption desorption at -196°C.

Electrochemical characterization: Electrochemical characterization procedures, comprising Cyclic Voltammetry (CV), Galvanostatic Charge Discharge (GCD), and Electrochemical Impedance Spectroscopy (EIS), were employed to estimate electrochemical behavior of the sample. These assessments were conducted on a Corrtest CS350 electrochemical workstation. The assessment was conducted in a three-electrode cell configuration, with the active material deposited onto nickel foam substrates. A mercury/mercury oxide electrode served as the reference electrode in a 3 M potassium hydroxide (KOH) electrolyte, while a platinum was employed as the auxiliary electrode.

For the preparation of the working electrode, initially, 1 mg of Polyvinylidene fluoride (PVDF) binder and 1 mg of carbon black were agitated in an agate mortar. To this, 8 mg of the activated carbon was added and then ground to make a homogeneous mixture, which was then loaded onto the nickel foam (1 × 1 cm^2) using propan-2-ol as a dispersant by drop casting method. The coated nickel foam was dried at 80 °C for 12 hours, resulting in an active mass loading of 5 mg. This prepared electrode was utilized for subsequent electrochemical testing. Cyclic-Voltammetry (CV) and galvanostatic charge-discharge (GCD) data were accomplished within a potential window of -1 to 0 V at various scan rates to assess the capacitive behavior of the material.

RESULTS AND DISCUSSION

Activated carbon was synthesized from the bark of *Acacia catechu* employing zinc chloride as an activating agent and heating at three different temperatures (400, 600, 800°C) in a nitrogen atmosphere. This resulted in the formation of AC with augmented area of surface, enhanced adsorption ability, and boosted active sites for ion/electron interchange. The carbonization process involved the removal of volatile matter, etching away of some carbon in the form of CO_2 and the development of a 3D nanoporous carbon [20].

The $ZnCl_2$ activating agent played a crucial role in the formation of the activated carbon, as it acted as a dehydrating and sacrificing agent, removes moisture as well as etching away some carbon in the form of CO_2 and leaving behind a porous 3D carbon structure [21, 22]. Mixing of $ZnCl_2$ into the biochar leads reaction of Zn^{2+} with bio-molecules present in the precursor. As a result, volatile organic substances get removed [23, 24]. The Zn-C complex gets decomposed with the increased carbonization temperature, resulting into the evolution of ZnO, $ZnCl_2$, and H_2 as vapor, consequentially developing voids or pores on the carbonaceous material [25]. Due to the realization of micro- and mesopores on the carbon matrix, 3D nanoporous carbon with higher surface area was formed [26].

FTIR was employed to inspect the functional groups existing in the as-prepared activated carbon samples. The FTIR spectra of all the activated carbon samples are depicted in Fig. 1(a). The BZAC-0 sample exhibited a broad band between 3600 and 3300 $cm^{-1,}$ equivalent to the -O-H stretching vibrations of hydroxyl groups [27]. However, this band was absent in the other samples (BZAC-4, BZAC-6, and BZAC-8) due to the heat treatment process. During the carbonization process, the cellulose structures were broken down as the hydroxyl groups diminished with the formation of water vapor which results into the porous structure. All the active materials (BZAC-4, BZAC-6, and BZAC-8) showed characteristic peaks at 1594 cm^{-1}, 955 cm^{-1}, and 876 cm^{-1}, which are attributed to the C-N stretching, C=C stretching, and out-of-plane C-H bending vibrations, respectively [24, 28]. The band corresponding to the C-O stretching vibration around 1098 cm^{-1} in BZAC-0 was shifted to 1152 cm^{-1} for the other samples (BZAC-4, BZAC-6, and BZAC-8) due to the activation process at elevated temperatures. The absence of significant strong peaks associated with water molecules in these samples indicates that the heat treatment effectively removed water from the samples [29]. Compared to the other samples, the FTIR spectrum of BZAC-8 showed significant peaks in the 900-1620 cm^{-1} region, indicating the presence of sp^2 hybridized C=C bonds along with C=N and C-N functional groups [30]. The presence of aromatic and aliphatic C=C bonds suggest the graphitization of the carbon materials as a function of temperature.

X-ray diffraction (XRD) analysis was employed to inspect the phase pureness and crystallinity of the $ZnCl_2$-activated carbon samples. The resulting diffraction patterns provided insights into the structural characteristics of the constituents. The XRD patterns of the BZAC-4, BZAC-6, and BZAC-8 samples are presented in Fig. 1(b). The diffraction patterns exhibited broad peaks, which is a characteristic signature of amorphous carbon materials. The absence of sharp, well-defined peaks advocates the absence of any residual $ZnCl_2$, indicating the successful formation of pure carbon [31]. The XRD patterns revealed two distinct broad peaks. The broad peaks observed in the XRD patterns indicate the predominantly amorphous nature of the carbon materials, which is typical for activated carbons derived from biomass precursors. The first prominent broad peak was observed at approximately 23.96° (2θ value), corresponding to an inter-planar spacing (d spacing) of ~0.38 nm, which can be assigned to the (002) plane. The second broad peak was observed at 42.92° with a d-spacing of

~0.21 nm, analogous to the (100) plane [7]. This peak is a characteristic of the graphitic nature of carbon materials. The findings from the XRD analysis are in consistent with the results obtained from the FTIR spectroscopy, further supporting the graphitic structure and the absence of any impurities in the $ZnCl_2$-activated carbon samples [32].

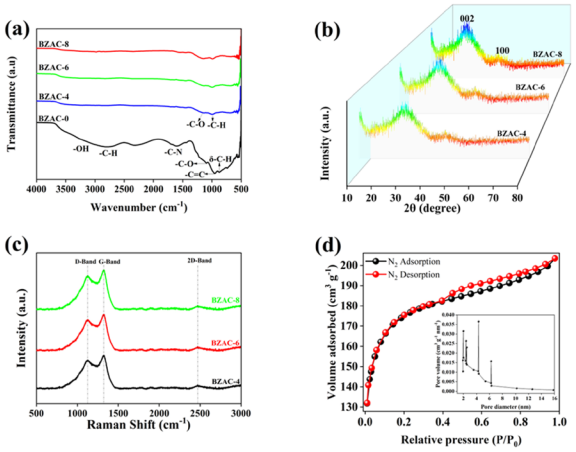

Fig. 1. Physicochemical characterization: (a) FTIR spectra, (b) XRD pattern, (c) Raman spectra, and (d) BET analysis illustrating N_2 adsorption-desorption (inset: pore size distribution) of BZAC-8.

Raman spectroscopic analysis was employed to further characterize the presence of defect and characteristic of carbon in the *Acacia catechu* bark-derived $ZnCl_2$ activated carbon samples. The Raman spectra were recorded in the range from 500 to 3000 cm^{-1} (λ = 514 nm), and the consequences are demonstrated in Fig.1(c). The Raman spectra of all three types of $ZnCl_2$ activated carbon samples exhibited a broad D band (defect-induced mode) centered around 1129 cm^{-1} and a G band (graphite E2g2 mode) at 1325 cm^{-1} [33]. The intensity ratio of the D band to the G band (I_D/I_G) was calculated for the BZAC-4, BZAC-6, and BZAC-8 samples, and the values were found to be 0.83, 0.92, and 0.96, respectively. These I_D/I_G ratios confirm the presence of a graphitic nature in the activated carbon, which is influenced by the temperature-dependent carbonization process. Furthermore, a prominent 2D band was observed at 2470 cm^{-1}, indicating a high degree of graphitization in the samples. The presence of this 2D band suggests that the *Acacia catechu* bark-derived $ZnCl_2$ activated carbon exhibits a well-developed graphitic structure [34].

The textural properties of the BZAC-8 activated carbon sample was investigated using nitrogen adsorption desorption at -196 °C. The Brunauer-Emmett-Teller (BET) technique was employed to determine the specific surface area of the sample. The BET plot for BZAC-8 (Fig. 1d) revealed an enhanced specific surface area of approximately 1947 $m^2\ g^{-1}$. The elevated carbonization temperature used in the preparation of BZAC-8 is likely to be contributed to the generation of a well-developed graphitic carbon structure, resulting in the observed high surface area. The nitrogen adsorption-desorption isotherm of BZAC-8 exhibited characteristics of a type II isotherm with a distinct hysteresis loop [35]. The presence of a steep increase in adsorption at low relative pressures ($P/P_0 < 0.2$) suggests the existence of micropores in the sample. Additionally, the hysteresis loop observed at higher relative pressures (P/P_0 from 0.4 to 1) indicates the presence of mesopores. The pore size distribution of BZAC-8, calculated using the Barrett-Joyner-Halenda (BJH) method, revealed pore sizes ranging from 2 to 6 nm. This combination of high specific surface area and the presence of both micropores and mesopores makes BZAC-8 a promising material for supercapacitor applications by providing efficient ion transport pathways and increased electrochemically active sites [36].

Field-Emission Scanning Electron Microscopy (FE-SEM) was used to observe the three-dimensional morphology of the BZAC samples. The obtained FE-SEM images revealed a porous structure, which is considered advantageous for efficient ion and electron conveyance processes. Fig. 2(a-i) presents the FE-SEM images along with EDX spectra of the BZAC samples. The FE-SEM analysis confirmed the presence of a porous network, even for the samples prepared at the lower carbonization temperature of 400°C (BZAC-4). Notably, the sample subjected to carbonization at 800°C (BZAC-8) exhibited a slight increase in the number of pores compared to BZAC-4 and BZAC-6. This interconnected porous structure of the BZAC-8 sample is likely to contribute to its enhanced specific capacitance performance. The development of this porous network can be attributed to the removal of various gaseous species (*e.g.*, CO_2, CO) and other compounds during the high-temperature chemical activation process [37]. The formation of these pores and channels provides improved accessibility to the active sites, facilitating efficient ion and electron transport within the electrode material [38].

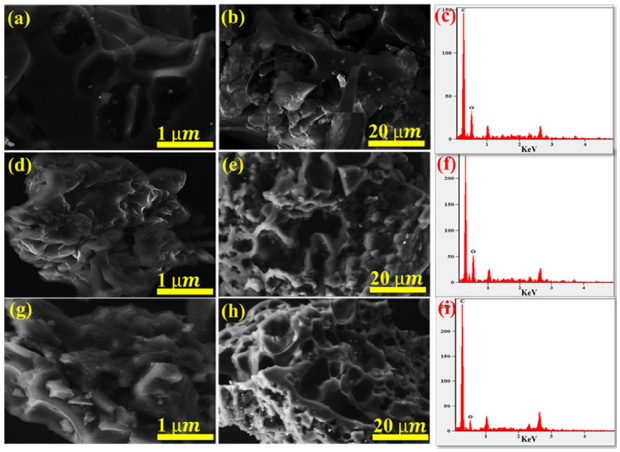

Fig. 2. Surface morphology and EDX study: FE-SEM images (a, b) of BZAC-4, (d, e) of BZAC-6, (g, h) of BZAC-8 at magnifications of 1 µm and 20 µm, respectively. (c, f, i) EDX of BZAC-4, BZAC-6 and BZAC-8, respectively.

Electrochemical Performance: The electrochemical properties of the BZAC samples were evaluated using a 3-electrode setup in a 3 M KOH solution. An Hg/HgO electrode served as the reference, while a platinum wire acted as the auxiliary electrode. The prepared BZAC material was used as the working electrode. Cyclic voltammetry (CV) was measured to assess the electrochemical behavior of BZAC samples. The potential window was ranged from -1.0 V to 0.0 V at various scan rates. The BZAC samples exhibited a negative electrode behavior due to the presence of surface functional groups. The CV curves of all the BZAC samples displayed an approximately rectangular shape, characteristic of electrical double-layer capacitor (EDLC) behavior [39]. Fig. 3(a), (d), and (g) signify the CV curves for the BZAC-4, BZAC-6, and BZAC-8 samples, correspondingly, at several scan rates (5-150 mV s^{-1}). With rise in scan rate, the area under the CV curve also augmented, specifying an upsurge in the current response [40]. Materials with higher surface area and a uniform porous structure tend to exhibit higher capacitive properties, as they can offer extra electrochemically active sites for charge storage. The area under the CV curve of BZAC-8 sample is found to be maximum compared to other indicating its superior capacitive behavior [5].

Fig. 3(b), (e), and (h) depict the galvanostatic charge-discharge (GCD) curves for the BZAC-4, BZAC-6, and BZAC-8 samples, respectively. The GCD curves exhibit a linear charging and discharging pattern characteristic of an EDLC behavior, devoid of any distinct oxidation-reduction peaks [41]. The GCD curves reveal that the BZAC-8 sample exhibits a longer discharging time compared to the other samples, demonstrating a greater specific capacitance. The specific capacitances of BZAC-8 were determined to be 377.15, 259.34, 208.8, 173.04, 165.52, 144.25, and 91 F g^{-1} at a current density of 0.5, 1, 2, 3, 4, 5 and 10 A g^{-1}, respectively. The specific capacitance for the BZAC-4, and BZAC-6 were found to be 235.55, 204.26, 179.36, 167.64, 144.68, 139.40, and 73.60 F g^{-1}, and 106.19, 95.85, 90.4, 88.72, 84.96, 68.95, and 44 F g^{-1}, respectively, at same current density. The BZAC-8 sample is characterized by a smaller internal resistance (IR) drop, which can be accredited to its well-connected porous network structure. The uniform and nanoporous structure, along with the graphitic nature of the active materials, contributes to the overall supercapacitive performance. The higher temperature carbonization of the biomass precursor leads to the graphitization of the carbon structure, transforming it from a predominantly sp^3 to sp^2 hybridization, as confirmed by the FTIR analysis. This structural transformation enhances the electrical conductivity and charge storage capacity of the activated carbon material [42].

The long-term electrochemical stability and Coulombic efficiency of the BZAC samples were evaluated through extended galvanostatic charge-discharge cycling. Fig. 3(c), (f), and (i) depict the cycling performance of the BZAC-4, BZAC-6, and BZAC-8 electrodes, respectively.

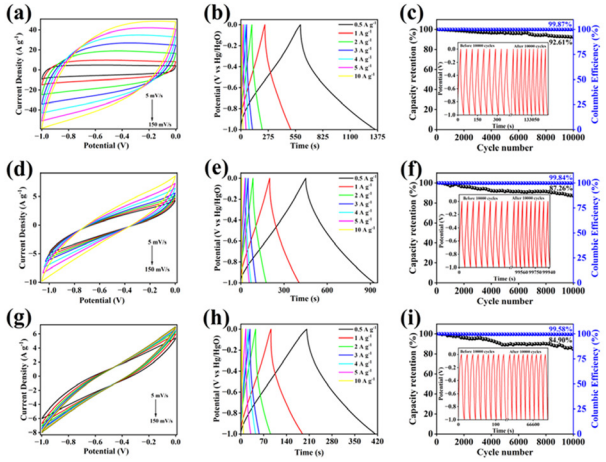

Fig. 3. Electrochemical characterization: (a, d, g) CV plots at scan rates of 5-150 mV s^{-1}, (b, e, h) GCD plots at different current densities and (c, f, i) Capacity retention and Coulombic efficiency of BZAC-8, BZAC-6 and BZAC-4, respectively.

The BZAC-8 electrode exhibited superb cyclic steadiness, retaining 92.61 % of its initial capacitance after 10,000 charge-discharge cycles. The Coulombic efficiency of the BZAC-8 electrode was maintained at 99.87 % throughout the cycling test. However, the BZAC-6 and BZAC-4 electrodes showed 87.26 % and 84.90 % capacity retention, respectively, along with Coulombic efficiencies of 99.84 % and 99.58 % after 10,000 cycles. The superior capacity retention of the BZAC-8 electrode can be attributed to its well-developed uniform micro- and mesoporous structure. This hierarchical pore network provides efficient ion transport pathways and accommodates volume changes during the charge-discharge process, thereby enhancing the enduring electrochemical constancy of the electrode material [43]. The stable cycling performance and high Coulombic efficiency of the BZAC-8 electrode demonstrate its excellent reversibility and robustness, which are crucial characteristics for practical supercapacitor applications.

Table 1. Summary of specific capacitance and capacity retention for various samples.

Sample	Specific Capacitance (F g^{-1}) at							C_{sp} retention (10000 cycles) (%)
	0.5 A g^{-1}	1 A g^{-1}	2 A g^{-1}	3 A g^{-1}	4 A g^{-1}	5 A g^{-1}	10 A g^{-1}	
BZAC-4	106.19	95.85	90.40	88.72	84.96	68.95	44.00	92.61
BZAC-6	235.55	204.26	179.36	167.64	144.68	139.40	73.60	87.26
BZAC-8	377.15	259.34	208.80	173.04	165.52	144.25	91.00	84.90

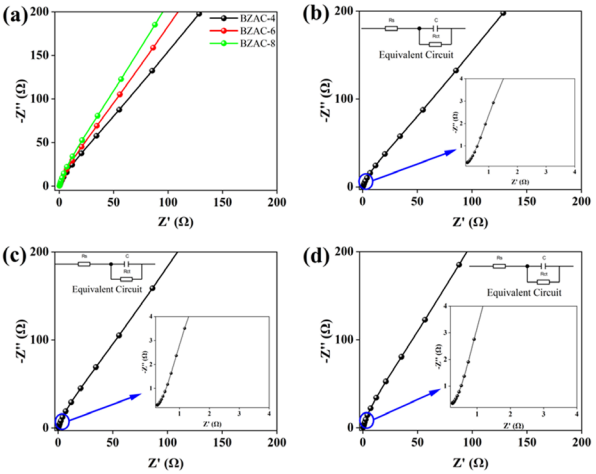

Fig. 4. Nyquist plots: (a) Comparative Nyquist plot of BZAC samples; (b) Nyquist plot of BZAC-4; (c) Nyquist plot of BZAC-6; and (d) Nyquist plot of BZAC-8 with equivalent circuit.

The optimized textural properties and the graphitic nature of the BZAC-8 sample contribute to its outstanding electrochemical cycling stability compared to the other BZAC samples.The specific capacitance at various current density and capacity retention of different BZAC sample after 10,000 charging-discharging cycles are illustrated in Table 1.

Electrochemical-impedance spectroscopy (EIS) was utilized to explore the resistive behavior of the electrode materials. The EIS measurements were conducted in the frequency ranging from 100 kHz to 1 mHz with an amplitude of 10 mV.

The comparative Nyquist plots for the BZAC samples are presented in Fig. 4(a) and Nyquist plot for BZAC-4, BZAC-6, BZAC-8 are shown in Fig. 4 (b-d), respectively with equivalent circuit.

The EIS spectra obtained from the Nyquist plots can be divided into several distinct regions comprising; the electrolytic resistance (Rs), which represents the resistance of the electrolyte solution, the semi-circle region attached to the x-axis, which corresponds to the charge transfer resistance (Rct) at the electrode-electrolyte interface, the middle region, which is somewhat horizontally inclined and represents the Warburg impedance (W), indicating diffusion-controlled processes, the vertically inclined region at low frequencies, which exhibits a capacitive nature, suggesting the presence of double-layer capacitance [44]. The experimentally obtained EIS data were fitted using an equivalent circuit model to extract the relevant electrochemical parameters. The electrode BZAC-8 displayed lower resistive behavior compared to the other BZAC-6, BZAC-4 samples. The Rct and Rs values for BZAC-8 were found to be 1.81 Ω and 1.37 Ω, respectively, while for BZAC-6 and BZAC-4, they were 1.96 Ω, 1.78 Ω, and 2.14 Ω, 1.92 Ω, respectively, as determined using Z view software.

These results suggest that the BZAC-8 electrode exhibits improved electron transfer kinetics and lower resistive behavior, which could be attributed to its structural and compositional characteristics. The EIS analysis provides valuable insights into the charge transfer processes occurring at the electrode-electrolyte interface and helps in understanding the electrochemical performance of the materials, which suggest BZAC-8 as a potential electrode material for supercapacitor application.

Table 2. Overview of biomass for supercapacitors, comparing capacitance, stability under given experimental conditions, and applicability of current research to supercapacitor applications.

S.N.	Source of biomass	Activating agent	Maximum capacitance (F g^{-1})	Capacitance at current density of	Electrolyte used	Cyclic Stability (cycles)	Reference
1	Soybean	KOH	220	0.5 Ag^{-1}	6 M KOH	99.2% (10000)	[45]
2	Sawdust	H_3PO_4	244.1	1 Ag^{-1}	1 M H_2SO_4	87% (10000)	[46]
3	Agave leaves	K_2CO_3	205	5 mV s^{-1}	1M Na_2SO_4	-	[47]
4	*Camellia oleifera* Shells	$ZnCl_2$	266	0.2 Ag^{-1}	6 M KOH	91.3% (5000)	[48]
5	Potato waste residue	$ZnCl_2$	255	0.5 Ag^{-1}	2 M KOH	93.7% (5000)	[49]
6	*Acacia catechu* bark	$ZnCl_2$	259.34	1 A g^{-1}	3 M KOH	92.61	This work

Table 2 demonstrates the comparative overview of various biomass used to prepare electrode materials for the supercapacitor devices utilizing different activators. *Acacia catechu* bark derived activated carbon spectacles the best result, with high capacitance and good stability over 10,000 charging-discharging cycles. This indicates it a promising material for supercapacitor electrodes.

CONCLUSION

This research explored the efficacy of exploiting waste *Acacia catechu* bark for the production of nanoporous activated carbon via a straightforward chemical activation process employing $ZnCl_2$ as the activating agent. The synthesized activated carbon materials were subjected to characterization using FTIR, XRD, Raman spectroscopy, BET analysis, and SEM. The electrochemical performance was appraised in a three-electrode with 3 M KOH electrolyte. A comparative analysis revealed that sample BZAC-8 exhibited superior gravimetric capacitance of 259.34 F g^{-1} at a current density of 1 A g^{-1}. This capacitance was accompanied by lower resistive behavior compared to samples BZAC-6 (204.26 F g^{-1}) and BZAC-4 (95.85 F g^{-1}) under the same current density. The enhanced supercapacitive performance observed in BZAC-8

can be directly accredited to the increment of micro and mesopores on the activated carbon's surface, as evidenced by the characterization techniques employed. In a nutshell, the outcomes of this work firmly recommend that sample BZAC-8 retains exceptional potential as a negative electrode material for supercapacitor applications. The combination of waste biomass utilization, a facile synthesis method, and the demonstrated superior electrochemical performance substantiates the promise of this material for future energy storage applications.

ACKNOWLEDGMENTS

This research work is supported by the University Grants Commission, Nepal (Award No. PhD78/79-S&T-04).

CONFLICT OF INTEREST

The writers proclaim no conflicts of interest, economic or personal, that could have potentially prejudiced the research presented in this manuscript.

REFERENCES

1. Park S., Song J., Lee W.C., Jang S., Lee J., *et al.* (2023) Advances in biomass-derived electrode materials for energy storage and circular carbon economy. *Chem. Eng. J.,* **470**, 144234. https://doi.org/10.1016/j.cej.2023.144234
2. Gogotsi Y., Patrice S. (2008) Materials for electrochemical capacitors. *Nat. Mater.*, **7**, 845-54. https://doi.org/10.1038/nmat2297
3. Simon P., Gogotsi Y., Dunn B. (2014) Where do batteries end and supercapacitors begin. *Science* **343**, 1210-1. https://doi.org/10.1126/science.1249625
4. Awasthi G.P., Bhattarai D.P., Maharjan B., Kim K.S., Park CH., Kim C.S. (2019) Synthesis and characterizations of activated carbon from Wisteria sinensis seeds biomass for energy storage applications. *J. Ind. Eng. Chem.*, **72**, 265-72. https://doi.org/10.1016/j.jiec.2018.12.027
5. Shrestha K.R., Kandula S., Rajeshkhanna G., Srivastava M., Kim NH., Lee JH. (2018) An advanced sandwich-type architecture of MnCo2O4@N-C@MnO2 as an efficient electrode material for a high-energy density hybrid asymmetric solid-state supercapacitor. *J. Mater. Chem. A*, **6**, 24509-22. https://doi.org/10.1039/c8ta08976k
6. Muzaffar A., Ahamed M.B., Deshmukh K., Thirumalai J. (2019) A review on recent advances in hybrid supercapacitors: Design, fabrication and applications. *Renew. Sustain. Energy Rev.*, **101**, 123-45. https://doi.org/10.1016/j.rser.2018.10.026
7. Rawat S., Mishra R.K., Bhaskar T. (2022) Biomass derived functional carbon materials for supercapacitor applications. *Chemosphere*, **286**, 131961. https://doi.org/10.1016/j.chemosphere.2021.131961
8. Chen X., Paul R., Dai L. (2017) Carbon-based supercapacitors for efficient energy storage. *Natl. Sci. Rev.*, **4**, 453-89. https://doi.org/10.1093/nsr/nwx009
9. Conway B.E., Pell W.G, (2003) Double-layer and pseudocapacitance types of electrochemical capacitors and their applications to the development of hybrid devices. *J. Solid State Electrochem.*, **7**, 637-44. https://doi.org/10.1007/s10008-003-0395-7
10. Dhakal G., Kumar D.R., Sahoo S., Shim J. (2003) Litchi seed biowaste-derived activated carbon supporting matrix for efficient symmetric and asymmetric supercapacitors. *Carbon*, **208**, 277-89. https://doi.org/10.1016/j.carbon.2023.03.045
11. Kar K.K. (2020) Handbook of nanocomposite supercapacitor *materials. I*, **300** https://doi.org/10.1007/978-3-030-43009-2_13
12. Shrestha R.L., Chaudhary R., Shrestha T., Tamrakar BM., Shrestha R.G., *et al.* (2020) Nanoarchitectonics of Lotus seed derived nanoporous carbon materials for supercapacitor applications. *Materials*, **13**, 5434. https://doi:10.3390/ma13235434
13. Mishra P.K., Shrestha K.R., Oli H.B., Shrestha T., Joshi L.P., *et al.* (2024) High-performance porous activated carbon derived from Acacia catechu bark as nanoarchitectonics material for supercapacitor applications. *J. Taiwan. Inst Chem. Eng.*, **165**, 105761. https://doi.org/10.1016/j.jtice.2024.105761
14. Xu Y., Lei H., Qi S., Ren F., Peng H., Wang F., *et al.* (2020) Three-dimensional zanthoxylum Leaves-Derived nitrogen-Doped porous carbon frameworks for aqueous supercapacitor with high specific energy. *J. Energy Storage*, **32**. https://doi.org/10.1016/j.est.2020.101970
15. Wang Y., Qu Q., Gao S., Tang G., Liu K., He S., *et al.* (2019) Biomass derived carbon as binder-free electrode materials for supercapacitors. *Carbon*, **155**, 706-26. https://doi.org/10.1016/j.carbon.2019.09.018
16. Brandão A.T.S.C., State S., Costa R., Potorac P., Vázquez J.A., *et al.* (2023) Renewable carbon materials as electrodes for high-performance supercapacitors: From marine biowaste to high specific surface area porous biocarbons. *ACS Omega*, **8**, 18782-98. https://doi.org/10.1021/acsomega.3c00816
17. Khan A., Arumugam S.R., Pan J., Sun Y., Liu X. (2020) Hierarchically porous biomass carbon derived from natural withered rose flowers as high-performance material for advanced supercapacitors. *Batter Supercaps*, **3**, 731-7 https://doi.org/10.1002/batt.202000046
18. Kunwar R.M., Shrestha K.P., Bussmann R.W. (2010) Traditional herbal medicine in Far-west Nepal: A pharmacological appraisal. *J. Ethnobiol.*

Ethnomed., **6**, 35. https://doi.org/10.1186/1746-4269-6-35
19. Adhikari B., Aryal B., Bhattarai B.R. (2021) A Comprehensive review on the chemical composition and pharmacological activities of Acacia catechu (L.f.) Willd. *J. Chem.,* https://doi.org/10.1155/2021/2575598
20. Gnawali C.L., Shrestha L.K., Hill J.P., Ma R., Ariga K., *et al.* (2023) Nanoporous activated carbon material from terminalia chebula seed for supercapacitor application. *C-Journal Carbon Res.*, **9**. https://doi.org/10.3390/c9040109
21. Li B., Hu J., Xiong H., Xiao Y. (2020) Application and properties of microporous carbons activated by ZnCl2: Adsorption behavior and activation mechanism. *ACS Omega*, **5**, 9398-407. https://doi.org/10.1021/acsomega.0c00461
22. Farma R., Julita R.I., Apriyani I., Awitdrus A., Taer E. (2023) ZnCl2-assisted synthesis of coffee bean bagasse-based activated carbon as a stable material for high-performance supercapacitors. *Mater. Today Proc.*, **87**, 25-31. https://doi.org/10.1016/j.matpr.2023.01.370
23. Altuntaş B.D,, Nevruzoğlu V., Dokumacı M., Cam Ş. (2020) Synthesis and characterization of activated carbon produced from waste human hair mass using chemical activation. *Carbon Lett.*, **30**, 307-13. https://doi.org/10.1007/s42823-019-00099-9
24. Köse K.Ö., Pişkin B., Aydınol M.K. (2018) Chemical and structural optimization of ZnCl2 activated carbons via high temperature CO_2 treatment for EDLC applications. *Int. J. Hydrogen Energy*, **43**, 18607-16. https://doi.org/10.1016/j.ijhydene.2018.03.222
25. Bosch D., Back J.O., Gurtner D., Giberti S., Hofmann A., Bockreis A. (2022) Alternative feedstock for the production of activated carbon with ZnCl2: Forestry residue biomass and waste wood. *Carbon Resour. Convers.*, **5**, 299-309. https://doi.org/10.1016/j.crcon.2022.09.001
26. Liu S., Dong K., Guo F., Wang J., Tang B., *et al.* (2024) Facile and green synthesis of biomass-derived N, O-doped hierarchical porous carbons for high-performance supercapacitor application. *J. Anal. Appl. Pyrolysis*, **177**, 106278. https://doi.org/10.1016/j.jaap.2023.106278
27. Ţucureanu V., Matei A., Avram A.M. (2016) FTIR Spectroscopy for carbon family study. *Crit. Rev. Anal. Chem.*, **46**, 502-20. https://doi.org/10.1080/10408347.2016.1157013
28. Setyaningrum D.L., Riyanto S., Rohman A. (2013) Analysis of corn and soybean oils in red fruit oil using FTIR spectroscopy in combination with partial least square. *Int. Food Res. J.*, **20**, 1977-81.
29. Wu H.Y., Chen S.S., Liao W., Wang W., Jang M.F., *et al.* (2020) Assessment of agricultural waste-derived activated carbon in multiple applications. *Environ. Res.*, **191**, 110176. https://doi.org/10.1016/j.envres.2020.110176
30. Shrestha D., Maensiri S., Wongpratat U., Lee S.W., Nyachhyon A.R. (2019) Shorea robusta derived activated carbon decorated with manganese dioxide hybrid composite for improved capacitive behaviors. *J. Environ. Chem. Eng.*, **7**, 103227. https://doi.org/10.1016/j.jece.2019.103227
31. Adhikari S., Subedi K., Dhungana S., Arhyal R.L., Paudyal H., *et al.* Chemical modification of banana peels and banana pseudostem for the adsorptive removal of chromium (VI) from aqueous solution. *J. Nepal. Chem. Soc.*, **43**, 23-33. https://doi.org/10.3126/jncs.v43i2.53338
32. Wang J., Nie P., Ding B., Dong S., Hao X., Dou H., *et al.* (2017) Biomass derived carbon for energy storage devices. *J. Mater. Chem. A*, **5**, 2411-28. https://doi.org/10.1039/c6ta08742f
33. Escribano R., Sloan J.J., Siddique N., Sze N., Dudev T. (2001) Raman spectroscopy of carbon-containing particles. *Vib. Spectrosc.*, **26**, 179-86. https://doi.org/10.1016/S0924-2031(01)00106-0
34. López-Díaz D., Delgado-Notario J.A., Clericò V., Diez E., Merchán M.D., Velázquez M.M. (2020) Towards understanding the Raman spectrum of graphene oxide: The effect of the chemical composition. *Coatings*, **10**, 1-12. https://doi.org/10.3390/COATINGS10060524
35. Dhakal G., Mohapatra D., Kim Y.Il., Lee J., Kim W.K., *et al*. (2022) High-performance supercapacitors fabricated with activated carbon derived from lotus calyx biowaste. *Renew. Energy,* **189**, 587-600. https://doi.org/10.1016/j.renene.2022.01.105
36. Dhakal G., Kumar D.R., Sahoo S., Shim J.J. (2023) Litchi seed biowaste-derived activated carbon supporting matrix for efficient symmetric and asymmetric supercapacitors. *Carbon,* **208**, 277-89. https://doi.org/10.1016/j.carbon.2023.03.045
37. Yang V., Senthil R.A., Pan J., Khan A., Osman S., *et al.* (2019) Highly ordered hierarchical porous carbon derived from biomass waste mangosteen peel as superior cathode material for high performance supercapacitor. *J. Electroanal. Chem.*, **855**, 113616. https://doi.org/10.1016/j.jelechem.2019.113616
38. Jung S.H., Myung Y., Kim B.N., Kim I.G., You I.K. (2018) Activated biomass-derived graphene-based carbons for supercapacitors with high energy and power density. *Sci. Rep.*, **8**, 1-8. https://doi.org/10.1038/s41598-018-20096-8
39. Zardkhoshoui A.M., Ashtiani M.M., Sarparast M., Hosseiny D.S.S. (2020) Enhanced the energy density of supercapacitors via rose-like nanoporous ZnGa2S4 hollow spheres cathode and yolk-shell FeP hollow spheres anode. *J. Power Sources,* **450**, 227691. https://doi.org/10.1016/j.jpowsour.2019.227691

40. Sun T., Liu Y., Xu D., Xu G., Ding Y., *et al.* (2023) Boosting supercapacitor performance through the facile synthesis of boron and nitrogen co-doped resin-derived carbon electrode material. *Diam. Relat. Mater.*, **138**, 110258. https://doi.org/10.1016/j.diamond.2023.110258
41. Cai P., Zou K., Deng X., Wang B., Zou G. (2020) Defect rich hierarchical porous carbon for high power supercapacitors, *Frontiers in Chemistry,* **8**, 1–11. https://doi.org/10.3389/fchem.2020.00043
42. Chae J. S, Kang W.S., Roh K.C. (2021) Sp2–sp3 hybrid porous carbon materials applied for supercapacitors. *Energies*, **14**, 1-9. https://doi.org/10.3390/en14195990
43. Dodevski V., Janković B., Stojmenović M., Krstić S., Popović J., *et al.* (2017) Plane tree seed biomass used for preparation of activated carbons (AC) derived from pyrolysis. *Modeling the Activation Process*. **522**. https://doi.org/10.1016/j.colsurfa.2017.03.003
44. Abdel Maksoud M.I.A., Fahim R.A., Shalan A.E., Elkodous A.M., Olojede S.O., *et al.* (2020) Advanced materials and technologies for supercapacitors used in energy conversion and storage: a review. *Springer International Publishing,* 19. https://doi.org/10.1007/s10311-020-01075-w
45. Jiao S., Yao Y., Zhang J., Zhang L., Li C., *et al.* (2023) Nano-flower-like porous carbon derived from soybean straw for efficient N-S co-doped supercapacitors by coupling in-situ heteroatom doping with green activation method. *Appl. Surf. Sci.,* **615**, 156365. https://doi.org/10.1016/j.apsusc.2023.156365
46. Zhou Y., Li J., Hu S., Qian G., Shi J., *et al.* (2022) Sawdust-derived activated carbon with hierarchical pores for high-performance symmetric supercapacitors. *Nanomaterials,* **12**, 810. https://doi.org/10.3390/nano12050810
47. Lobato-Peralta D.R., Ayala-Cortés A., Longoria A., Pacheco-Catalán D.E., Okoye P.U., *et al.* (2022) Activated carbons obtained by environmentally friendly activation using solar energy for their use in neutral electrolyte supercapacitors. *Journal of Energy Storage,* **52**. https://doi.org/10.1016/j.est.2022.104888
48. Zhang J., Gong L., Sun K., Jiang J., Zhang X. (2012) Preparation of activated carbon from waste Camellia oleifera shell for supercapacitor application. *J. Solid State Electrochem.,* **16**, 2179-86. https://doi.org/10.1007/s10008-012-1639-1
49. Ma G., Yang Q., Sun K., Peng H., Ran F., *et al.* (2015) Nitrogen-doped porous carbon derived from biomass waste for high-performance supercapacitor. *Bioresource Technology,* **197**, 137-42. https://doi.org/10.1016/j.biortech.2015.07.100